MEMS, Field-Emitter, Thermal, and Fluidic Devices

A Compact Flash X-Ray Source Based Upon Silicon Field Emitter Arrays

W. Chern[1], G. Rughoobur[1], N. Karaulac[1], A. Kramer[2], R. Gupta[2], A. I. Akinwande[1]
1. Massachusetts Institute of Technology (MIT), 2. Massachusetts General Hospital (MGH)
Sponsorship: AFOSR

X-rays are used for non-destructive imaging in virtually every industry today. They enable doctors to make diagnostic decisions to quality assurance for electronics and industrial components. The machines that do these tasks are large, bulky, and occasionally slow due to the design of the X-ray system. Every X-ray imaging system is generally limited to up to 2 X-ray sources due to the cost but primarily the size. The majority of commercial X-ray sources are based upon thermionic emission or a heated filament similar to that of an incandescent light bulb. Because of the high temperature of the thermionic source, it is difficult to shrink the size of the X-ray tube. Field emission is a solution that has been touted for decades, but it has always had reliability problems. We resolve these problems by demonstrating that a high-performance and potentially compact flash X-ray source can be realized. The current X-ray setup, completed in collaboration with Massachusetts General Hospital (MGH) and shown in Figure 1, has been shown to be reliable enough to take hundreds of images for computed tomography to reconstruct a 3D image. These X-rays were taken in pulsed mode, where short bursts of a few hundred nanoseconds are used to turn the field emitter on, the first demonstration of its kind.

▲Figure 1: Rotating computed tomography (CT) setup at MGH based upon Si field emitters. The sample rotates to enable images being taken at different angles. The inset show the view inside the chamber where Si FEAs are mounted on a vacuum feedthrough and contacted through wirebonds. The devices sit 1.5 cm away from a Mo anode cut at 45 degrees.

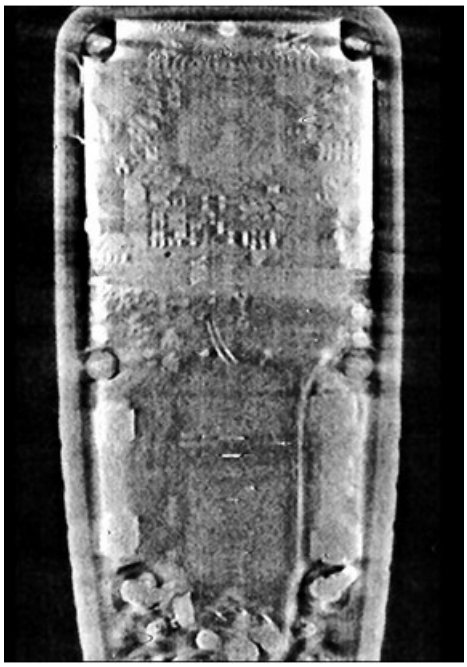

▲Figure 2: Vertical slice from a CT reconstruction showing the cross-section of a multimeter at the board level. The components of the board are clearly visible in the image.

A Silicon Field Emitter Array as an Electron Source for Phase-controlled Magnetrons

W. Chern, J. Browning, A.I. Akinwande
Sponsorship: AFOSR

Magnetrons are a highly efficient (>90%), high-power vacuum-based microwave source. In a magnetron, free electrons in vacuum are subject to a magnetic field while moving past open metal cavities, resulting in the emission of resonant microwave radiation. Current state-of-the-art magnetrons use a heated metal filament to thermionically emit electrons into vacuum continuously and are not addressable. This work seeks to replace the heated metal filament as a source of electrons with Si field emitter arrays to improve efficiency and increase power, especially when several sources are combined. Si field emitter arrays, schematically shown in Figure 1, are devices that are normally off and are capable of high current densities plus spatial and temporal addressing. These arrays consist of many sharp Si tips sitting on long Si nanowires that limit the current of the electron emission. Electrons from the Si tips tunnel into a vacuum as a result of the high electric field of the applied bias on the polysilicon gate. Pulsing the electric field applied on the gate can turn the arrays on and off. The proposed use of Si field emitter arrays in a magnetron will allow injection locking and hence phase control of magnetrons. Phase-controlled magnetrons have multiple applications in areas where high-power microwave sources are desired. Currently, Si field emitter arrays have been designed for the magnetron; our collaborators at Boise State University are testing them.

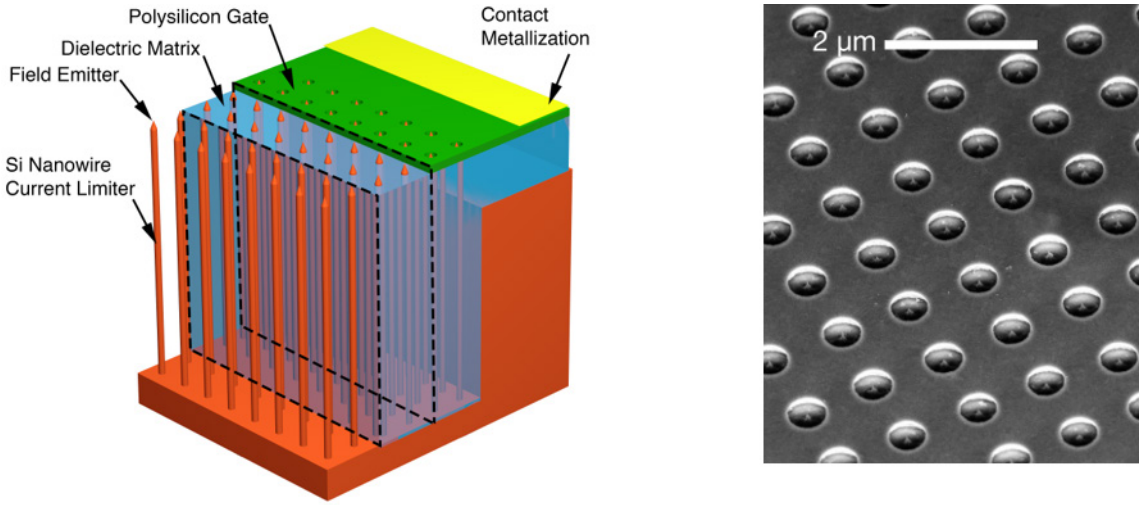

▲ Figure 1: (Left) 3-D rendering of Si device structure. For clarity, layers have been omitted in different regions of the rendering to show detail. In the front, the bare Si nanowires [200-nm diameter & 10-µm height] with sharp tips. (Right) Top view of a fabricated device with 350-nm gate aperture and 1-µm tip-to-tip spacing.

FURTHER READING

- S. Guerrera and A. I. Akinwande, "Silicon Field Emitter Arrays with Current Densities Exceeding 100 A/cm2 at Gate Voltages Below 75 V," in *Proceedings of IEDM*, 2016.

Acoustically-active Surface for Automobile Interiors Based on Piezoelectric Dome Arrays

J. Han, J. Lang, V. Bulović
Sponsorship: Ford Motor Inc.

The surfaces of automobile interiors can be rendered acoustically active by mounting on them thin, wide-area membranes with arrays of small acoustic transducers. Each small, individually addressable transducer functions as a speaker or a microphone, and an entire pixelated acoustic membrane enables directional sound generation and sensing. The frequency response of the wide-area acoustically-active surface is determined by those of the small isolated acoustic transducers, which thereby yields better tunability of the bandwidth through designing pixel dimensions. As a result, the acoustically-active surface can work either in the audio frequency range for noise cancellation, personal entertainment, and communication with the vehicle, or - in the ultrasonic frequency range - for gesture detection, alertness monitoring, etc., which collectively improve the comfort and safety of the automobiles.

This project seeks to develop and demonstrate a thin, wide-area acoustic "wallpaper" based on an array of dome-shaped piezoelectric transducers, which exhibits outstanding performance and is deemed the most suitable option for miniaturization and scalable fabrication. Dependencies of device performance for both speaker and microphone applications on the material properties, dome dimensions, and back cavity structure have been studied through theoretical modeling and numerical simulation. For speaker applications, a 12-μm thick, 8-inch wafer-size acoustic wallpaper consisting of an array of PVDF domes that are sub-1-mm in diameter is capable of generating over 60 dBSPL a half meter away with a 1-kHz, 10-V driving voltage, which can be further enhanced by scaling up the area and reducing the thickness of the membrane. On the other hand, reducing the radius of PVDF domes will lead to an extended bandwidth into the ultrasound range at a small cost of sound pressure level in the audio frequency range. We have developed a scalable process to fabricate such acoustic wallpapers. A 1×1 cm^2 sample (Figure 1) has been fabricated for demonstration and will be scaled up to a 10×10 cm^2 wallpaper to explore prospective applications of acoustically active surfaces.

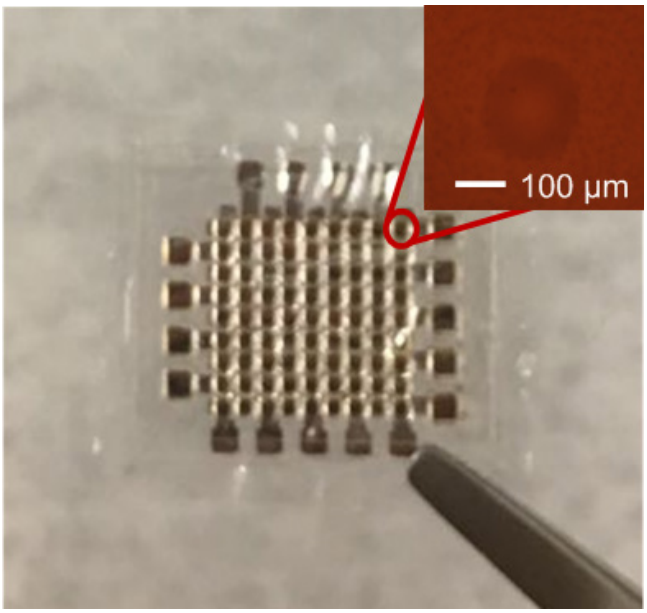

▲ Figure 1: A 1×1 cm^2 sample of the acoustic membrane with individually addressable acoustic transducers based on embossed PVDF domes. The inset shows a close-up scan of a single PVDF dome.

The Scanning Anode Field Emission Microscope: A Tool for Mapping Emission Characteristics of Field Emitter Array Devices and Structures

O. O. Ilori, A. I. Akinwande
Sponsorship: Air Force Office of Scientific Research

We developed a scanning anode field emission microscope (SAFEM) for characterizing field emission array (FEA) devices and structures (see Figure 1). The SAFEM is designed to accurately and precisely scan and position a probing anode tip over emitter tips of an FEA and acquire maps of emitter tip current $I_E(x,y)$ and anode-to-emitter voltage $V_{AE}(x,y,)$ from which the map of spatial variation of the field factor $\beta(x,y)$ and the distribution $f(\beta)$ are extracted. The scanning and positioning movement is achieved by using two positioning stages. The first stage holds the device so a sample can move in the xyz direction with a travel range of 26 mm and resolution of 6 nm. The second stage holds the probing anode and can also move in the xyz direction with a travel range of 5 mm and a resolution of 0.03 nm. Its probing and imaging of emission currents from FEA devices and structures enable use of the SAFEM to observe the aging, i.e., temporal evolution of FEA devices in vacuum and gas ambient, and to measure accurately the turn-on and operating voltage of FEA devices. The SAFEM is operational and has been used to obtain current maps of various FEA devices, as in Figure 2. Images obtained by the SAFEM have been used to optimize the fabrication of FEAs for high-current and long-lifetime operations.

The resolution of the SAFEM is determined by scan step size, relative sizes of emitter tip radii (r_E), anode tip radius (r_A), and emitter array pitch (T_P): $r_E << r_A << T_P$. To obtain a well-resolved current map of FEA tips, the SAFEM is operated in the pulsed mode. The scanning motion, voltage (or current) sourcing, and current (or voltage) measuring functions of the SAFEM can be independently operated in either a pulsed or continuous mode. In the completely pulsed mode, the scanning anode moves a discrete scan step and enters a wait state long enough for the movement response to reach steady state. Once the steady state is reached, the source measure unit turns on the anode voltage and waits for the emission current response to also reach a steady value before the command to measure the current is issued. The duty cycles of the pulsing operation are critical to obtaining a well resolved current map. Operation in the pulsed mode significantly reduces the described noise current from the FEA substrate, nearby edges, nearby tips, and stage movements compared to other modes of operation.

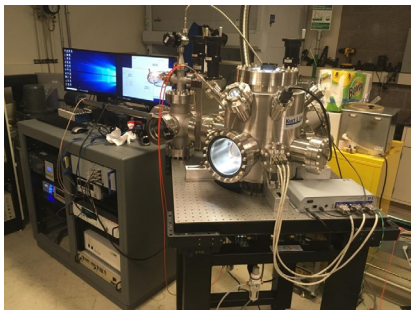

◀ Figure 1: The completed SAFEM instrumentation.

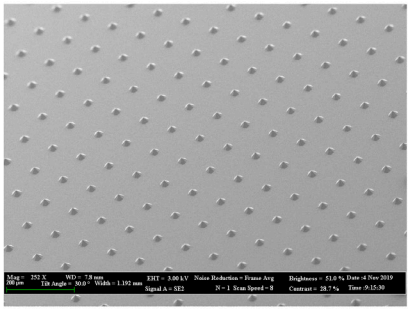

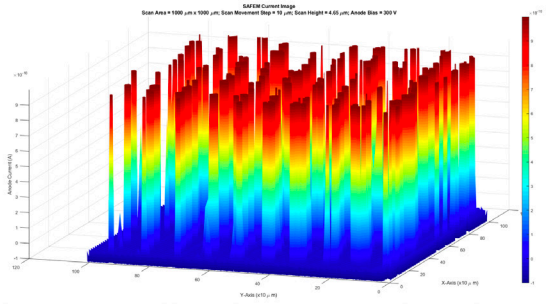

▼ Figure 2: Test FEA device and corresponding current image.

FURTHER READING

- L. Nilsson, O. Groening, P. Groening, O. Kuettel, and L. Schlapbach, "Characterization of Thin Film Electron Emitters by Scanning Anode Field Emission Microscopy," *J. of Applied Physics*, vol. 90, no. 2, pp. 768–780, Jul. 2001.
- T. Wang, C. E. Reece, and R. M. Sundelin, "Direct Current Scanning Field Emission Microscope Integrated with Existing Scanning Electron Microscope," *Review of Scientific Instruments*, vol. 73, no. 9, pp. 3215–3220, Sep. 2002.
- F. Andrianiazy, J.-P. Mazellier, L. Sabaut, L. Gangloff, P. Legagneux, and O. Gröning, "Quantitative Characterization of Field Emission Parameters: Application to Statistical Analysis of Individual Carbon Nanotubes/nanofibers," *J. of Vacuum Science & Technology B*, vol. 33, no. 1, p. 012201, Nov. 2014.

Highly Uniform Silicon Field-Emitter Arrays

N. Karaulac, A. I. Akinwande
Sponsorship: DARPA, IARPA

Cold cathodes based on silicon field-emitter arrays (FEAs) have shown promise in a variety of applications requiring high-current-density electron sources. However, FEAs face a number of challenges that have prevented them from achieving widespread use in commercial and military applications. One problem limiting the reliability of FEAs is emitter tip burnout due to Joule heating. The current fabrication process for FEAs results in a non-uniform distribution of emitter tip radii. At a fixed voltage, emitters with a small radius emit a higher current while emitters with a large radius emit a lower current. Therefore, emitters with a small radius reach their thermal limit due to Joule heating at lower voltages and consequently burn out. Previous solutions to mitigating tip burnout have focused on limiting the emitter current with resistors, transistors, or nanowires in order to obtain a more uniform emission current.

In this project, we focused on increasing the uniformity of emitter tip radii as a means to reduce tip burnout. Figure 1 shows a typical distribution of emitter tip radii for FEAs. The non-uniform distribution of emitter tip radii first forms during the photolithography step that defines the array of "dots" that become the etching mask for the silicon tips. In our FEA fabrication process, we used a trilevel resist process that nearly eliminated the light wave reflected at the photoresist/silicon interface and hence improved the uniformity of the dot diameter. Furthermore, we integrated the emitter tips with silicon nanowires to improve their reliability. Figure 2 shows a diagram of the fabricated structure. Our fabrication process resulted in FEAs with a more uniform emission current and a potentially longer lifetime.

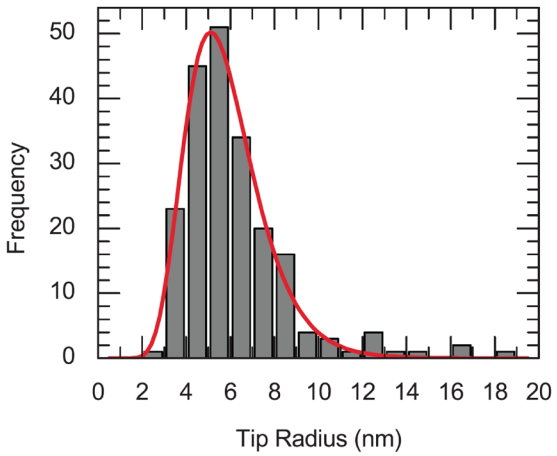

▲Figure 1: Non-uniform distribution of emitter tip radii resulting from the fabrication of silicon FEAs.

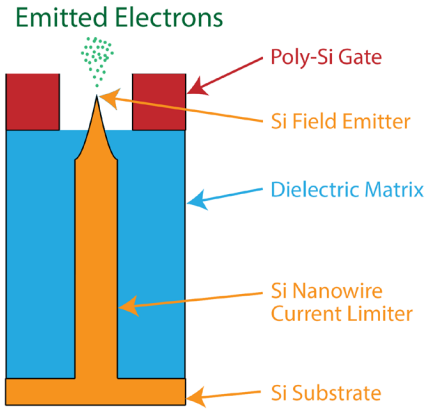

▲Figure 2: Cross-sectional diagram of a silicon field emitter. The emitter tip sits on top of a high-aspect ratio silicon nanowire that limits the field emission current from the tip.

FURTHER READING

- S. A. Guerrera, and A. I. Akinwande, "Nanofabrication of Arrays of Silicon Field Emitters with Vertical Silicon Nanowire Current Limiters and Self-Aligned Gates," *Nanotechnology*, vol. 27, no. 29, pp. 295302:1-11, Jul. 2016.
- M. L. Schattenburg, R. J. Aucoin, and R. C. Fleming, "Optically Matched Trilevel Resist Process for Nanostructure Fabrication," *Journal of Vacuum Science & Technology B: Microelectronics and Nanometer Structures*, vol. 13, no. 6, p. 3007, Nov. 1995.

CMOS Opto-nanofluidics

J. Kim, H. S. Lee, R. J. Ram
Sponsorship: Kwanjeong Educational Foundation, Bose Foundation

CMOS (complementary metal-oxide-semiconductor) foundries offers designers access to nanometer scale patterns, a suite of readout and interface circuits, and, more importantly, the capability to mass-manufacture their designs. These features of microelectronic CMOS foundries have been extensively utilized for photonic applications. This abstract introduces their application to opto-nanofluidics.

In MicroTAS 2017, we first reported the process of fabricating nanofluidic channels inside CMOS chips by defining the channels using the polysilicon gate layer and releasing the channels by sacrificial etching. Since then, we developed a packaging approach to accommodate mm-sized dies, which are the norm in multi-project wafer runs. The CMOS opto-nanofluidic chip in Figure 1 was fabricated in a 65-nm SOI CMOS process (10LP+) with integrated photodetectors.

The packaging approach employs a low-cost epoxy material to extend the die area and a back-side machining step to planarize and thin the wafer down for subsequent lithography and etch steps. The I-V curves in Figure 2 indicate that the photodetectors are fully operational after the substrate extension and nanochannel release. Future chips will include an integrated amplifier with 0.6 μV/√Hz simulated input referred noise for improved sensitivity by lock-in detection. We plan to apply this CMOS opto-nanofluidic platform for single-molecule manipulation and sensing applications.

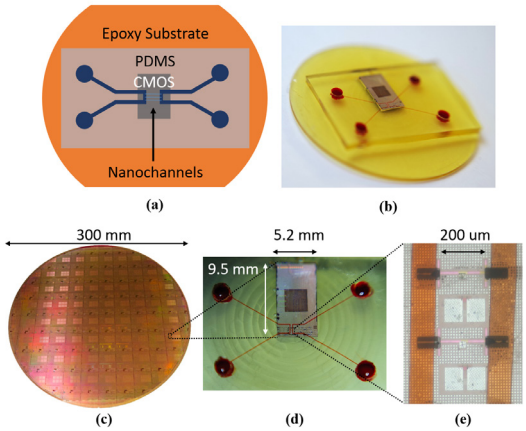

▲Figure 1: (a) Schematic of packaged CMOS opto-nanofluidic chip, (b) Photograph of chip, (c) Full 65- nm SOI wafer, (d) Packaged chip with PDMS micro-channels, (e) Micrograph of opto-nanofluidic devices.

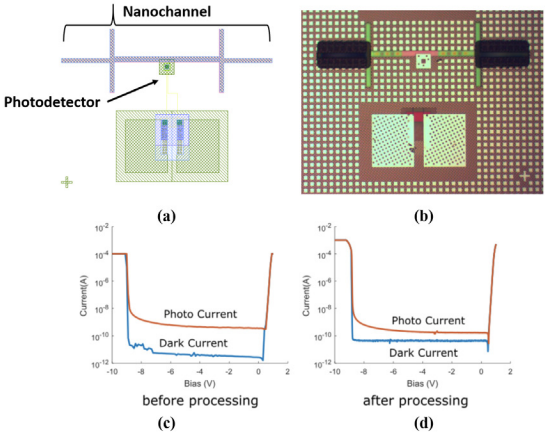

▲Figure 2: (a) CAD layout of nanochannel with integrated photodetector, (b) Micrograph of fabricated device, (c) I-V curves of photodetector before and (d) after nanochannel processing.

FURTHER READING

- H. Meng, J. Kim, A. Atabaki, and R. J. Ram, "Integration of Nanofluidics with Microelectronic CMOS," *Proc. 21st International Conference on Minaturized Systems for Chemistry and Life Sciences*, p. 788, Oct. 2017.
- J. Kim, H. Meng, and R. J. Ram, "Post-processing Compatible Packaging Method for CMOS Opto-nanofluidic Chip," *Proc. 23rd International Conference on Miniaturized Systems for Chemistry and Life Sciences*, p. 1074, Oct. 2019.
- T. Datta-Chaudhuri, P. Abshire, and E. Smela, "Packaging Commercial CMOS Chips for Lab on a Chip Integration," *Lab on a Chip*, vol. 14, no. 10, pp. 1753-1766, Mar. 2014.

Increasing the Yield of Atmospheric Pressure Microsputtering for Fabrication of Agile Electronics

Y. Kornbluth, R. Matthews, L. Parameswaran, L. M. Racz, L. F. Velásquez-García
Sponsorship: U.S. Air Force

Additive manufacturing (AM) promises new, flexible production; however, while AM excels at creating structural parts, it cannot make functional objects well, e.g. multi-material structures such as electronic components and circuits. Sputtering, which removes material from a target atom-by-atom by using a plasma, is used in IC fabrication finely layered, multi-material fabrication. By miniaturizing the dimensions of the plasma reactor down to sub-millimeter scale, the sputterer can operate at atmospheric pressure, obviating the need for a vacuum. However, at atmospheric pressure, collisions with gas molecules scatter most of the sputtered material, preventing it from reaching the substrate.

We develop plasma microsputterer technology that allows for high-resolution, high-quality deposition of arbitrary patterns, without any templates, pre-, or post-processing; recent results with a gold target include creating imprints with electrical conductivity within an order of magnitude to that of bulk metal. We explore two methods to minimize sputtered material scattering and to increase the deposition rate (yield). The first method minimizes the gap between the sputtering target and the substrate (Fig. 1): the sputtering target is placed 150 µm above the substrate. Dielectric barriers confine the plasma, forcing the plasma to connect the target wire and anode without damaging the substrate. This approach yields 0.2 nm/s (40 pg/s)—twice previous results. However, significant substrate heating occurs, which is incompatible with temperature-sensitive substrates. The second method harnesses convection to drive the sputtered material towards the substrate (Fig. 2). We surround the microsputter target (100 µm diameter) with a strong jet of air (100 m/s, 0.5 mm thick coaxial flow) to force air molecules to transport the sputtered material. This method greatly increases the yield (1 nm/s, 20 ng/s)—30% of the sputtered material reaches the substrate. Current work focuses on further increasing the deposition rate by increasing the rate at which atoms are sputtered.

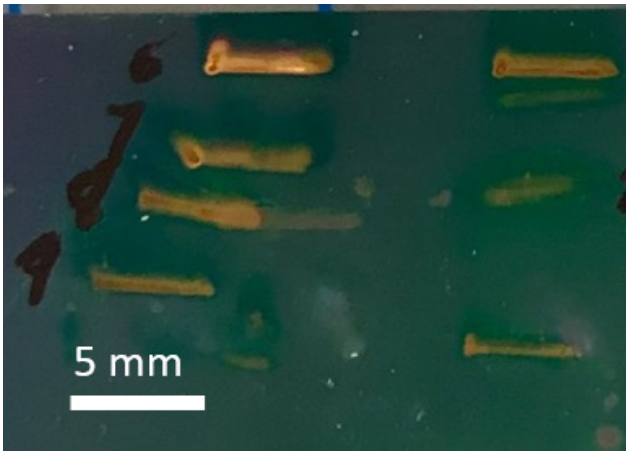

▲Figure 1: A set of lines printed on a substrate using a gold microsputterer with a small gap (150 µm) between the target and the substrate.

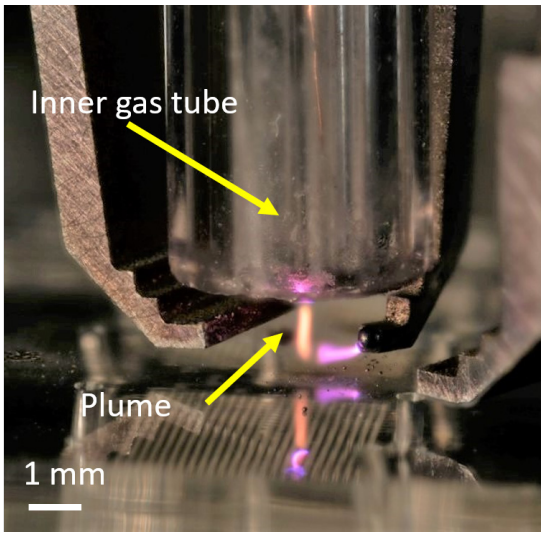

▲Figure 2: Setup with coaxial gas plume; the gas plume (orange) carries ionized air and sputtered gold down to the substrate. We cannot detect any meaningful substrate heating. The purple parts of the plasma are due to high argon and gold content in those areas.

FURTHER READING

- Y. Kornbluth, R. H. Mathews, L. Parameswaran, L. M. Racz, and L. F. Velásquez-García, "Room-temperature, Atmospheric-pressure Microsputtering of Dense, Electrically Conductive, Sub-100 nm Gold Films," *Nanotechnology*, vol. 30, no. 28, p. 285602, Apr. 2019.
- Y. Kornbluth, R. H. Mathews, L. Parameswaran, L. M. Racz, and L. F. Velásquez-García, "Microsputterer with Integrated Ion-drag Focusing for Additive Manufacturing of Thin, Narrow Conductive Lines," *Journal of Physics D – Applied Physics*, vol. 51, no. 16, p. 165603, Apr. 2018.

Silicon MEMS Compatible Bipropellant Micro Rocket Engine Using Steam Injector

J. Protz
Sponsorship: Protz Lab Group; microEngine, LLC; Asteria Propulsion, LLC

Rocket engines miniaturized and fabricated using MEMS or other techniques have been an active area of research for two decades. At these scales, miniaturized steam injectors like those used in Victorian-era steam locomotives are viable as a pumping mechanism and offer an alternative to pressure feed and high-speed turbo-pumps. Storing propellants at low pressure reduces tank mass, and this improves the vehicle empty-to-gross mass ratio; if one propellant is responsible for most of the propellant mass (e.g., oxidizer), injecting it while leaving the others solid or pressure-fed can still achieve much of the potential gain. Previously, the principal investigator and his group built and tested ultraminiature-machined micro jet injectors that pumped ethanol and also explored liquid and, more recently, hybrid engine designs. Recent work has focused on designing and implementing a whole-engine test article that simultaneously integrates a steam injector, boiler, decomposition chamber, fuel injector and thrust chamber, that is practical to build, and that is compatible with MEMS fabrication. An axisymmetric engineering mockup in brass was built to demonstrate the feasibility of the design concept (see Figure 1). Configurations that combine electrically-driven pumps with steam injectors by, for example, using electric pumps to pump fuel or coolant and a steam injector motivated by boiled coolant to pump oxidizer are also being explored. These would allow pressurized tanks to be avoided altogether while still being compatible with miniaturization via MEMS.

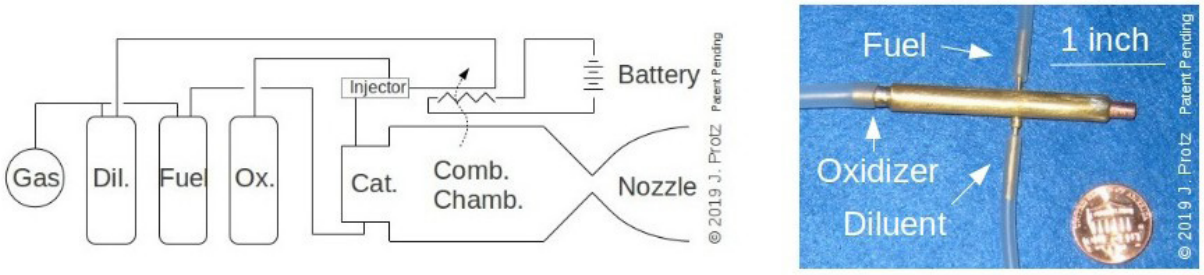

▲Figure 1: (a) Schematic representation of engine and (b) engineering mock-up in brass of a fully-integrated engine.

FURTHER READING

- J. Protz, "Hybrid and Partially Pressure-Fed Injector-Pumped Micro Rockets," (JANNAF 2019-004BT), presented at the *Joint Army-Navy-NASA-Air Force Joint Meeting of the 13th Modeling and Simulation / 11th Liquid Propulsion / 10th Spacecraft Propulsion Subcommittees and Meeting of the Programmatic and Industrial Base (JANNAF)*, Tampa, FL, Dec. 9-13, 2019.
- J. M. Protz, "Progress Towards an Injector-pumped Micro Rocket Engine and Vehicle," invited talk to *Gas Turbine Laboratory*, MIT, Cambridge, MA, May 7, 2019.
- J. M. Protz, "Modeling and Analysis of a Giffard-injector-pumped Bipropellant Microrocket," invited talk to *Pratt & Whitney Rocketdyne*, Huntsville, AL, February 3, 2010.

Gated Silicon Field Ionization Arrays for Compact Neutron Sources

G. Rughoobur, A. I. Akinwande
Sponsorship: DARPA

Neutron radiation is widely used in various applications, ranging from the analysis of the composition and structure of materials and cancer therapy to neutron imaging for security. However, most applications require a large neutron flux that is often achieved only in large infrastructures such as nuclear reactors and accelerators. Neutrons are generated by ionizing deuterium (D_2) to produce deuterium ions (D^+) that can be accelerated towards a target loaded with either D or tritium (T). The reaction generates neutrons and isotopes of He, with the D-T reaction producing the higher neutron yield. Classic ion sources require extremely high positive electric fields, on the order of 108 volts per centimeter (10 V/nm). Such a field is achievable only in the vicinity of sharp electrodes under a large bias; consequently, ion sources for neutron generation are bulky.

This work explores, as an alternative, highly scalable and compact Si field ionization arrays (FIAs) with a unique device architecture that uses self-aligned gates and a high-aspect-ratio (~40:1) silicon nanowire current limiter to regulate electron flow to each field emitter tip in the array (Figure 1). The tip radius has a log-normal distribution with a mean of 5 nm and a standard deviation of 1.5 nm, while the gate aperture is ~350 nm in diameter and is within 200 nm of the tip. Field factors, β, > 1 × 10^6 cm-1 can be achieved with these Si FIAs, implying that gate-emitter voltages of 250-300 V (if not less) can produce D+ based on the tip field of 25-30 V/nm. In this work, our devices achieve an ionization current of up to 5 nA at ~140 V for D_2 at pressures of 10 mTorr. Gases such as He and Ar can also be ionized at voltages (<100 V) with these compact Si FIAs (Figure 2).

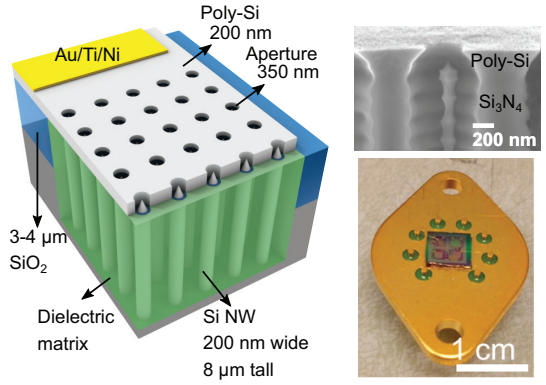

▲Figure 1: Schematic of gated field ionization array, with SEM cross-section of a single field ionizer and photograph of a packaged chip with arrays of different sizes for neutron generation.

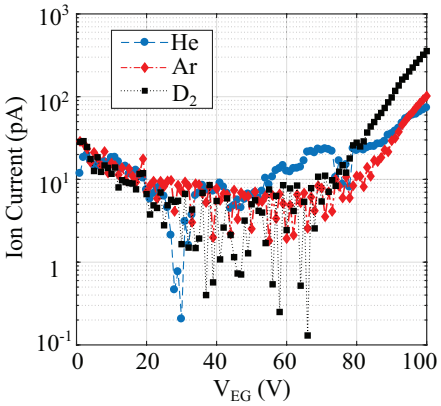

▲Figure 2: Ion current measured for different gases (He, Ar, and D_2) at 1 mTorr pressure demonstrating low ionization voltages using 1000 by 1000 Si FIAs.

FURTHER READING

- M. Araghchini, S. A. Guerrera, and A. I. Akinwande, "High Current Density MEMS Deuterium Ionizers," *2016 29th International Vacuum Nanoelectronics Conference*, pp. 1–2, 2016.
- A. Fomani, L. F. Velasquez-Garcia, and A. I. Akinwande, "Low-voltage Field Ionization of Gases up to Torr-level Pressures using Massive Arrays of Self-aligned Gated Nanoscale Tips," *IEEE Trans. Electron Devices*, vol. 61, no. 5, pp. 1520–1528, 2014.
- B. Johnson, P. R. Schwoebel, P. J. Resnick, C. E. Holland, K. L. Hertz, and D. L. Chichester, "Field Ionization Characteristics of an Ion Source Array for Neutron Generators," *J. Appl. Phys.*, vol. 114, no. 17, p. 174906, Nov. 2013.

Silicon Field Emitter Arrays (FEAs) with Focusing Gate and Integrated Nanowire Current Limiter

G. Rughoobur, Lay Jain, A. I. Akinwande
Sponsorship: AFRL, IARPA

The advent of microfabrication has enabled scalable and high-density Si field emitter arrays (FEAs). These are advantageous due to compatibility with complementary metal-oxide semiconductor (CMOS) processes, the maturity of the technology, and the ease in fabricating sharp tips using oxidation. The use of a current limiter is necessary to avoid burn-out of the sharper tips. Active methods using integrated MOS field-effect transistors and passive methods using a nano-pillar (~200-nm wide, 8-µm tall) in conjunction with the tip have been demonstrated. Si FEAs with single gates reported in our previous works have current densities of >100 A/cm2 and operate with lifetimes of over 100 hours.

The need for another gate (Figure 1) becomes essential to control the focal spot size of the electron beam as electrons leaving the tip have an emission angle of 12.5 . The focus electrode provides a radial electric field that reduces the lateral velocity of stray electrons and narrows the cone angle of the beam reaching the anode. Varying the voltage on the focus gate reduces the focal spot size or achieves an electron beam modulator for radio frequency applications. In this work, we fabricate dense (1-µm pitch) double-gated Si with an integrated nanowire current limiter (Figure 2). The apertures are ~350 nm and ~550 nm for the extractor and focus gates, respectively, with a 350-nm-thick oxide insulator separating the two gates. Electrical characterization of the fabricated devices shows that the focus-to-gate ratio (VFE/VGE) can be used to control the anode current (Figure 2). When the focus voltage exceeds the gate voltage, the field superposition increases the extracted current, and vice versa. These devices can potentially find applications as high-current focused electron sources in flat panel displays, nano-focused X-ray generation, and microwave tubes.

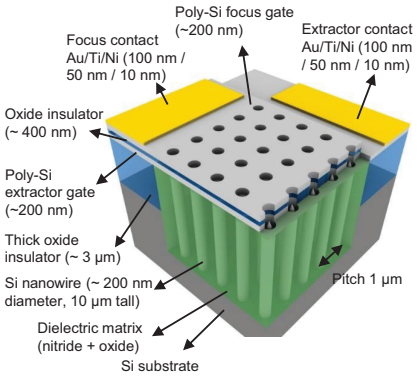

▲Figure 1: Si field emitter array with integrated current limiter, self-aligned extractor, and focus gates for nano-focused cold electron sources.

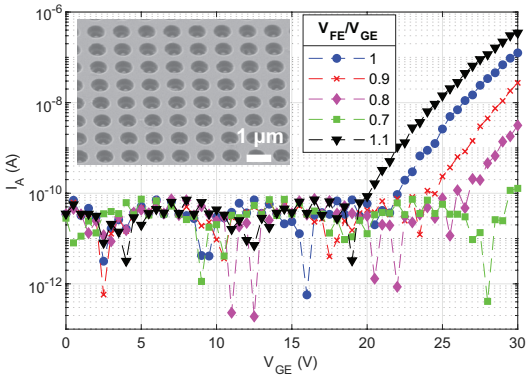

▲Figure 2: Electrical characterization of 500 x 500 arrays with different focus/gate voltage ratios at 1000 V anode; inset shows the fabricated double-gated array.

FURTHER READING

- S. A. Guerrera and A. I. Akinwande, "Nanofabrication of Arrays of Silicon Field Emitters with Vertical Silicon Nanowire Current Limiters and Self-aligned Gates," *Nanotechnology*, vol. 27, no. 29, p. 295302, Jul. 2016.
- L. Y. Chen and A. I. Akinwande, "Aperture-collimated Double-gated Silicon Field Emitter Arrays," *IEEE Trans. Electron Devices*, vol. 54, no. 3, pp. 601–608, 2007.
- L. Dvorson, I. Kymissis, and A. I. Akinwande, "Double-gated Silicon Field Emitters," J. *Vac. Sci. Technol. B Microelectron. Nanom. Struct.*, vol. 21, no. 1, p. 486, 2003.

Electron Transparent Anodes for Field Emission Cathodes in Poor Vacuum

G. Rughoobur, L. Jain, A. I. Akinwande
Sponsorship: AFOSR, Multidisciplinary University Research Initiatives

Nanoscale Vacuum Channel Transistors (NVCTs) using field emission sources could potentially have superior performance compared to solid state devices of similar channel length. This is due to ballistic transport of electrons, shorter transit time and higher breakdown voltage in vacuum. Furthermore, there is no opportunity for ionization or avalanche carrier multiplication imbuing NVCTs with very high Johnson figure of merit (~1014 V/s). However, field emitters need ultra-high vacuum (UHV) for reliable operation as the field emission process is sensitive to barrier height variations induced by adsorption/desorption of gas molecules. Small changes in the barrier height cause exponential variations in current. Poor vacuum also leads to generation of energetic ions that bombard the emitters, altering the work function and degrading electrical performance.

To overcome the UHV requirement, graphene can be used to nano-encapsulate the field emitter in UHV or a gas (e.g. He) with high ionization energy. Separation of the electron tunneling region from the electron acceleration region enables emission of electrons in UHV and electron transport in poor vacuum, if not atmospheric conditions. For mechanical strength, a multi-layer graphene structure that is transparent to electrons while being impervious to gas molecules/ions is necessary. In this work experimentally characterize the electron transparency of graphene membranes using arrays of gated Si field emitters with 1 μm pitch (Figure 1) that exhibit transistor-like characteristics. Using an energized multi-layer graphene/grid structure (Figure 2) in combination with emitter arrays, we measured extremely high electron yield perhaps due to secondary emission from electrons impinging on the graphene layer. Adopting this architecture for NVCTs will allow the realization of empty state electronics capable of functioning at higher frequencies (THz regime) higher power and harsher conditions (high radiation and high temperature) compared to solid state electronics.

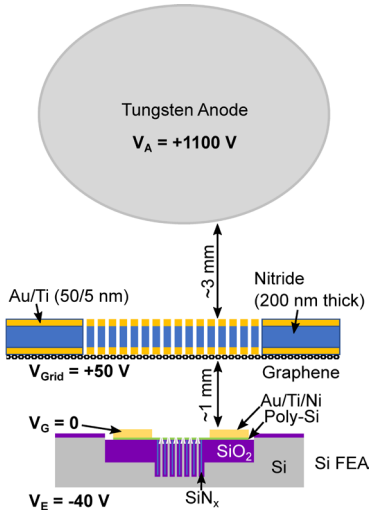

▲Figure 1: Schematic of measurement of graphene electron transparency at low electron energies with membranes of graphene layers.

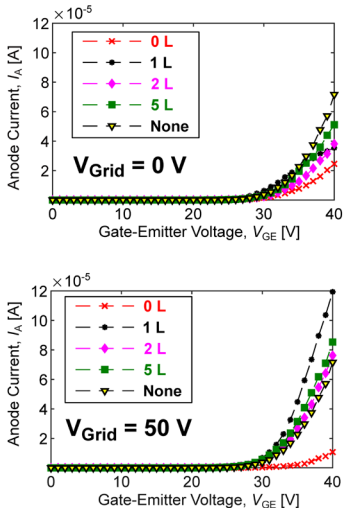

▲Figure 2: Anode current ratio (100 by 100 array) comparison with no acceleration (VGrid = 0 V) and acceleration of VGrid = 50 V for different number of layers on the membrane.

FURTHER READING

- S. A. Guerrera and A. I. Akinwande, "He Channel NanoTransistors — Towards 'Vacuum-less' Empty State Electronics," 2016 29th International Vacuum Nanoelectronics Conference, pp. 1–2, 2016.
- S. Bunch, S. S. Verbridge, J. S. Alden, A. M. Van Der Zande, J. M. Parpia, H. G. Craighead, and P. L. Mceuen, "Impermeable Atomic Membranes from 2008," Nano Lett., vol. 8, p. 2458–2462, 2008.
- J.-W. Han, D.-I. Moon, and M. Meyyappan, "Nanoscale Vacuum Channel Transistor," Nano Lett., vol. 17, no. 4, pp. 2146–2151, Apr. 2017

GaN Vertical Nanowires with Self-Aligned Gates for Field Emission Applications

P.-C. Shih, T. Palacios, in collaboration with G. Rughoobur, A. I. Akinwande
Sponsorship: AFOSR

Field emitters (FE), or namely vacuum transistors, are promising for harsh-environments and high-frequency electronics thanks to their radiation hardness and scattering-free electron transport. However, the stability and operating voltage still need improvement to enable circuit applications. To overcome these issues, III-Nitrides are excellent candidates due to their strong bonding energies and tunable electron affinities. Though the material properties of III-Nitrides are promising, so far, there are few works demonstrating sub-100 V turn on as most III-N FEs are still two-terminal structures.

In this work, we demonstrate a novel GaN nanowire (NW) FEs based on self-aligned gates to reduce the gate-emitter turn-on voltage (VGE, ON) below 30 V. The GaN on Si wafer was grown by Enkris Semiconductor, Inc. Thanks to a new GaN processing technology, we successfully fabricate GaN NWs with width of 60 nm and aspect-ratio of 5 (Figure 1 (a)). The gate stack is then conformally deposited. We then finish the device fabrication by dry etching to open FEs' tips (Figure 1 (b)).

We measure the transfer characteristics with a suspended 0.5-mm-diameter tungsten ball biased at +500 V as an anode (Fig. 2(a)). Device turns on at 27 V. This device demonstrates the lowest turn-on voltage among GaN field emitters in literature, as well as excellent current density (Fig. 2 (b)) and shows great potential for integrated circuit applications.

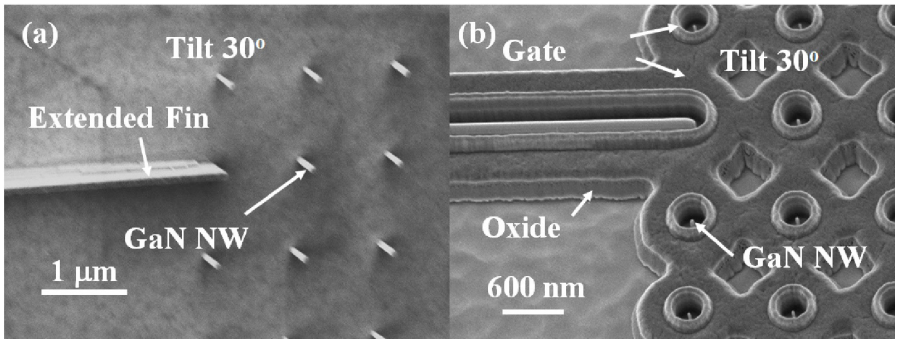

▲Figure 1: Scanning electron microscope (SEM) images of (a) GaN NWs with extended fin and (b) finished self-aligned gate FEs. The "extended fin" is used to connect the gate metal to a large metal pad.

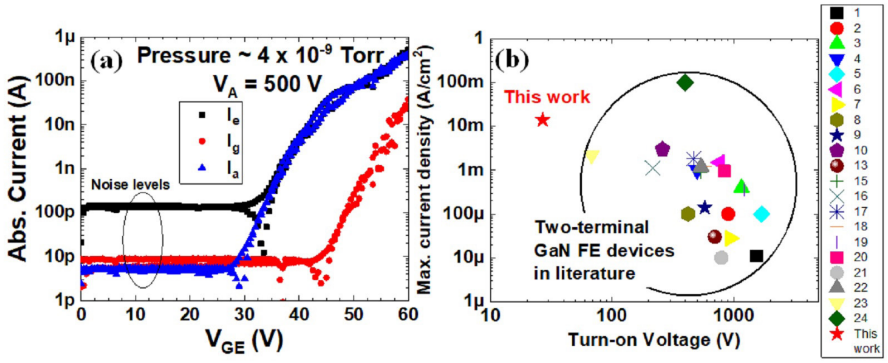

▲Figure 2: (a) Transfer characteristics of a 50 × 50 NW arrays with NW width of 60 nm and NW height of 300 nm. (b) Benchmark plot of different GaN FE devices.

FURTHER READING

- P.-C. Shih, G. Rughoobur, P. Xiang, K. Liu, K. Cheng, A. I. Akinwande, and T. Palacios, "GaN Nanowire Field Emitters with a Self-Aligned Gate Process," to be presented at *78th Device Research Conference*, Columbus, Ohio, June 2020.

3D-Printed, Miniature, Multi-material, Valve-less, Magnetically Actuated Liquid Pumps

A. P. Taylor, L. F. Velásquez–García
Sponsorship: Edwards Vacuum

Miniaturized pumps can be used to supply precise flow rates of liquid in compact systems. Numerous micro-fabricated positive displacement pumps for liquids with chamber volumes that are cycled using valves have been proposed. Pumps made via standard (i.e., cleanroom) micro-fabrication typically cannot deliver large flow rates without integrating hydraulic amplification or operating at high frequency due to their small pump chambers.

3D-Printing has recently been explored as a processing arena for microsystems; in particular, researchers have reported 3D printed pumps for liquids and gases with performance on par with or better than counterparts made with standard microfabrication.

Building on earlier work on printed magnetically actuated liquid pumps, we 3D-printed multi-material, magnetically driven, valve-less miniature liquid pumps. We used the fused filament fabrication (FFF) method: a thermoplastic filament is extruded from a hot nozzle to create, layer by layer, a solid object. The body of the pump is printed in Nylon 12, while the actuation magnet is printed in Nylon 12 containing NdFeB micro-particles. The devices are driven by a non-contact rotating magnet and employ valve-less diffusers to greatly simplify operation.

Our low-cost, leak-tight, miniature devices are microfabricated using 150- and 225-µm layers with a multi-step, multi-material printing process (Figure 1) that monolithically creates all key features with <13-µm in-plane misalignment. Each pump has a frame, a 225-µm-thick membrane connected to a piston with an embedded magnet, a chamber, two diffusers, and two fluidic connectors (Figure 2). Fabrication of the pump requires under 75 minutes and costs less than $3.89. Finite element analysis of the actuator predicts a maximum stress of 15.7 MPa @ 100 µm deflection, i.e., below the fatigue limit of Nylon 12 for infinite life (i.e., 19 MPa). Water flow rate up to 1.68 ml/min at an actuation frequency of 204 Hz was measured.

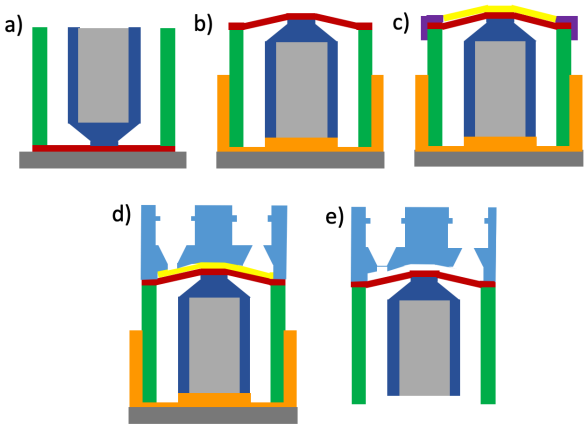

▲ Figure 1: Process flow to FFF-print liquid pump: a) print pump's membrane (red), piston (blue), frame (green), and magnet (gray). b) While membrane is warm, deform it using a mandrel (orange). c) Place shadow mask (purple) on membrane and apply PVAc film (yellow); d) Remove mask and print chamber ceiling, valves and fittings; e) Dissolve PVAc film.

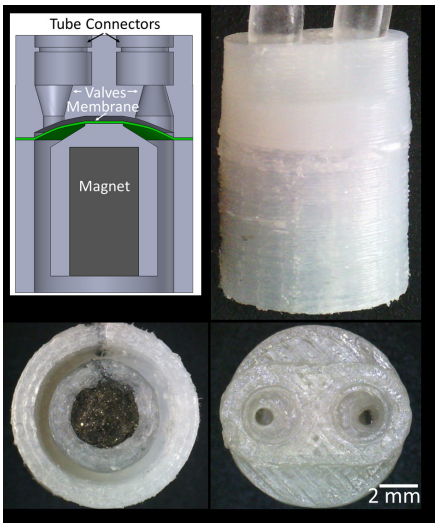

▲ Figure 2: Clockwise from top left: CAD model cross-section of pump; side view of printed pump; top view of printed pump; bottom view of printed pump showing the printed magnet. The scale bar applies to all printed objects.

FURTHER READING

- A. P. Taylor, C. Velez Cuervo, D. P. Arnold, and L. F. Velásquez–García, "Fully 3D-printed, Monolithic, Mini Magnetic Actuators for Low-cost, Compact Systems," *J. Microelectromech. Syst.* Vol. 28, no. 3, pp. 481–493, Jun. 2019.
- A. P. Taylor and L. F. Velásquez–García, "Low-cost, Monolithically 3D-printed, Miniature High-flow Rate Liquid Pump," *J. Phys. Conf. Ser.* vol. 1047, pp. 012040-44, Jul. 2019.
- A. P. Taylor and L. F. Velásquez–García, "Low-cost, Fully 3D-printed, Magnetically Actuated, Miniature Valve-less, Liquid Pump," *PowerMEMS 2019 Conference Proceedings*, Dec. 2019.

Measurement of the Condensation Coefficient of Water Using an Ultrathin, Nanoporous Membrane

G. Vaartstra, Z. Lu, J. Lee, J. C. Grossman, E. N. Wang
Sponsorship: NSF

In applications ranging from electronics cooling and power generation cycles to distillation, liquid-vapor phase change phenomena play a critical role. At their fundamental (kinetic) limits, evaporation and condensation are dictated by the resistance to molecules crossing the liquid-vapor interface, which is quantified by the condensation coefficient. Despite its fundamental importance and widespread use in heat transfer models such as the Schrage equation, the condensation coefficient of water has been difficult to characterize, with experimental results and theoretical calculations spanning three orders of magnitude. Experimental measurement has been challenging because three conditions must be satisfied: sensitivity to the condensation coefficient is high, temperature of the liquid-vapor interface is precisely yet noninvasively measured, and the concentration of contaminants at the liquid-vapor interface is low. To achieve a precise measurement of the condensation coefficient of water, we have fabricated an ultrathin (~200 nm), nanoporous (~150 nm diameter), hydrophobic membrane for forward-osmosis (FO) driven transport (Figure 1). Due to the ultrathin, low-aspect ratio dimensions of the membrane, we achieve high sensitivity to the condensation coefficient and avoid undesired contaminant buildup at the interface because the membrane is freestanding. Since transport is driven by osmotic pressure, the system can be maintained at isothermal conditions such that the temperature can be precisely measured in the bulk water without interfering with the liquid-vapor interface. These experimental measurements of the condensation coefficient of water are crucial for modeling liquid-vapor phase change in nanoscale systems and advanced thermal management devices.

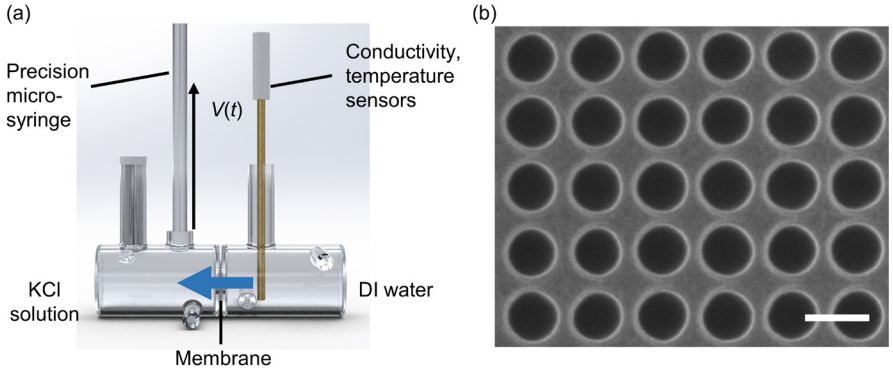

▲ Figure 1: (a) Schematic of the FO experiment. The blue arrow indicates the flux of water vapor across the hydrophobic membrane, which is measured by the volume change V(t) of liquid in the precision syringe. (b) SEM image of the nanoporous membrane, the scale bar is 200 nm.

FURTHER READING

- J. Lee, T. Laoui, and R. Karnik, "Nanofluidic Transport Governed by the Liquid/vapour Interface," *Nat. Nanotech.*, vol. 9, pp. 317-323, Apr. 2014.
- Z. Lu, I. Kinefuchi, K. L. Wilke, G. Vaartstra, and E. N. Wang, "A Unified Relationship for Evaporation Kinetics at Low Mach Numbers," *Nat. Commun.*, vol. 10, pp. 2368, May 2019.

In-plane Gated Field Emission Electron Sources via Multi-material Extrusion

I. A. Perales-Martínez, L. F. Velásquez-García
Sponsorship: MIT-Tecnologico de Monterrey Nanotechnology Program

Field emission is the quantum tunneling of electrons to vacuum due to local high electrostatic fields; such high fields can be generated at a moderate voltage using nanosharp, high-aspect-ratio tips. Compared to thermionic counterparts, field emission cathodes consume less energy, respond faster, and can operate in poorer vacuum, making them attractive in compact applications such as nanosatellite electric propulsion, portable mass spectrometry, and handheld X-ray generation. A wide variety of materials has been explored as field emitters; the research in field emission electron sources has focused on carbon nanotubes (CNTs) due to their nanosized tip diameter, high aspect-ratio, high electrical conductivity, and excellent chemical stability. However, most manufacturing methods for CNT field emission electron sources have associated large cost, long processing time, need of static masks for defining in specific locations the nanostructured emitting material and/or the electrode(s), and large gate interception (or the need for advanced assembly methods to attain high transmission).

In this project, we are developing low-cost field emission cathodes via multi-material extrusion. The devices are flat plates with two concentric imprints (Figure 1): an imprint made of CNTs (emitting electrode), symmetrically surrounded on both sides by an imprint made of Ag microparticles (extractor gate). Unlike the great majority of field emission cathodes reported that have an out-of-plane gate electrode, our devices have an in-plane gate that significantly reduces the cost and manufacturing complexity of the device and also facilitates high gate transmission. Our devices can emit electrons in vacuum with as little as 62 V applied between the CNT imprint and the Ag imprint and achieve over 97% gate transmission (Fig. 2). Current work focuses on increasing the imprint density to attain larger current density emission and on developing ballasting structures for attaining large and uniform array emission.

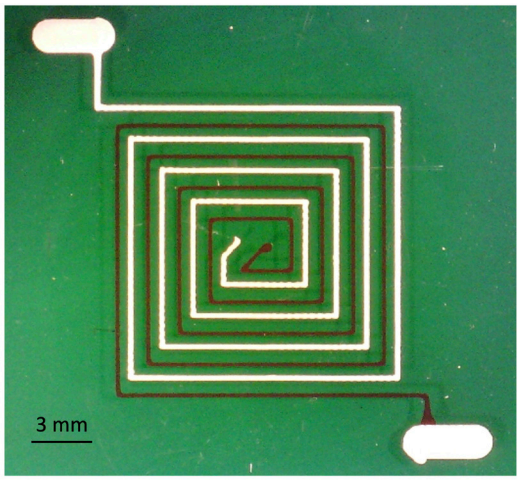

▲Figure 1: Optical top view of a square-loop field emission source with 700-μm pitch between adjacent traces

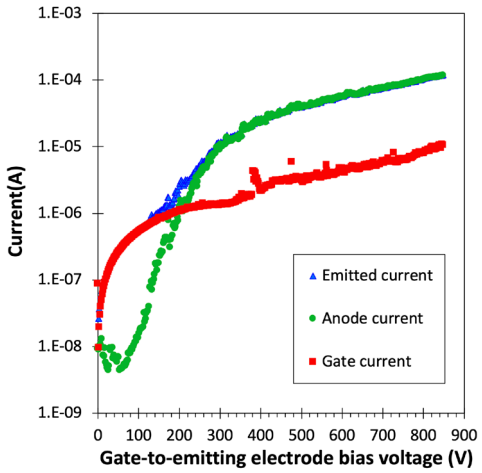

▲Figure 2: Emitted, gate, and collected currents vs. bias voltage for the device shown in Figure 1.

FURTHER READING

- I. A. Perales and L. F. Velásquez-García, "Fully 3D-Printed Carbon Nanotube Field Emission Electron Sources with In-plane Gate Electrode," *Nanotechnology*, vol. 30, no. 49, p. 495302, Dec. 2019.
- C. Yang and L. F. Velásquez-García, "Low-cost, Additively Manufactured Electron Impact Gas Ionizer with CNT Field Emission Cathode for Compact Mass Spectrometry," *Journal of Physics D – Applied Physics*, vol. 52, no. 7, p. 075301, Feb. 2019.
- L. F. Velásquez-García, A. I. Akinwande, and M. Martínez-Sánchez, "Precision Hand Assembly of MEMS Subsystems Using DRIE-patterned Deflection Spring Structures: An Example of an Out-of-Plane Substrate Assembly," *Journal of Microelectromechanical Systems*, vol. 16, no. 3, pp. 598 – 612, Jun. 2007.

Additively Manufactured, Miniature Electrohydrodynamic Gas Pumps

Z. Sun, L. F. Velásquez-García
Sponsorship: MIT-Skoltech Next Generation Program

A corona discharge is a self-sustained physical phenomenon induced around the sharper electrode of a diode due to sharply nonuniform electric fields within the interelectrode space. Ion propagation across such a space is accompanied by collisions with neutral particles, resulting in bulk fluid movement known as ionic wind. In contrast to traditional counterparts, ionic wind pumps have no moving parts, respond faster, and produce significantly less noise, drawing great interest in applications such as air propulsion and electronics cooling. Currently, ionic wind pump technology is far from practical in applications that require large flow velocity, flow rate, and power efficiency; another concern is the stability of the pump, given that ion accumulation in the interelectrode space can cause an electric short during sustained operation. Researchers have proposed using active electrodes with a plurality of field enhancers arranged in parallel (multiplexing) to maximize throughput; however, the reported multi-needle devices are serially assembled, and their performance is inferior to that of single-needle counterparts.

This project uses metal additive manufacturing and electropolishing to create miniature, multi-needle ionic wind pumps. Our devices are needle-ring corona diodes composed of a monolithic inkjet binder-printed active electrode (Figure 1), made in stainless steel 316L, with a plurality of sharp, conical needles and a thin plate copper counter-electrode, with electrochemically etched apertures aligned to the needle array. Five-needle ionic wind pumps eject air at 2.9 m/s and at a volumetric flow rate of 343 cm3/s, three times larger than the flow rate of a single-tip device with comparable efficiency (Figure 2). Current work systematically studies the relevant parameters to optimize the design of the electrohydrodynamic pump.

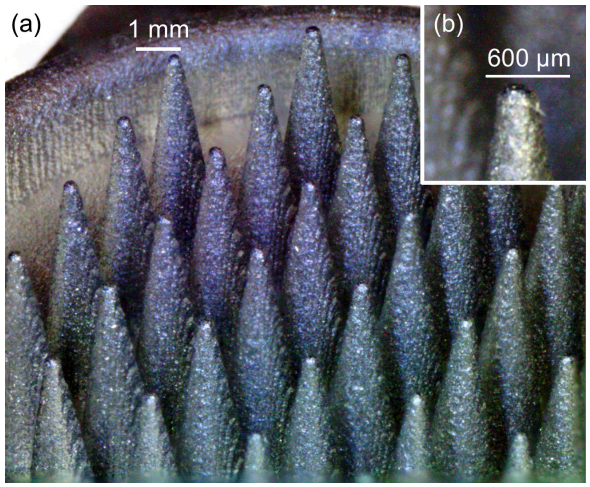

▲Figure 1: Field view (a) and tip close-up (b) of an as-printed 32-tip active electrode; the structure is binder inject-printed in stainless steel 316L.

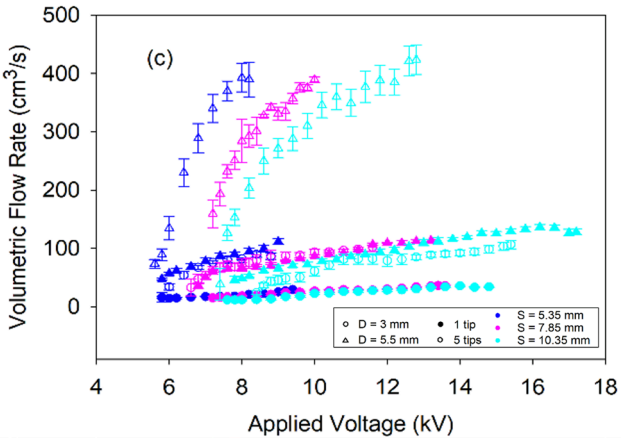

▲Figure 2: Volumetric flow rate vs. bias voltage for 1-needle and 5-needle ionic wind pumps with different counter-electrode aperture D and inter-electrode separation S.

FURTHER READING

- Z. Sun, G. Vladimirov, E. Nikolaev, and L. F. Velásquez-García, "Exploration of Metal 3-D Printing Technologies for the Microfabrication of Freeform, Finely Featured, Mesoscaled Structures," *Journal of Microelectromechanical Systems*, vol. 27, no. 6, pp. 1171 – 1185, Dec. 2018.
- Z. Sun and L. F. Velásquez-García, "Miniature, Metal 3D-Printed, Multiplexed Electrohydrodynamic Gas Pumps," *Plasma Research Express*, to be published, 2020. DOI: 10.1088/2516-1067/ab8f04
- L. F. Velásquez-García, A. I. Akinwande, and M. Martínez-Sánchez, "Precision Hand Assembly of MEMS Subsystems using DRIE-patterned Deflection Spring Structures: An Example of an Out-of-Plane Substrate Assembly," *Journal of Microelectromechanical Systems*, vol. 16, no. 3, pp. 598 – 612, Jun. 2007.

3D-Printed Silver Catalytic Microreactors for Efficient Decomposition of Hydrogen Peroxide

E. Segura-Cardenas, L. F. Velásquez-García
Sponsorship: MIT-Tecnologico de Monterrey Nanotechnology Program

Microreactors increase the surface-to-volume ratio of their reactants and by-products, resulting in faster, more efficient reactions and better heat transfer than in their non-miniaturized counterparts, leading to higher throughput per unit of reactor active volume and to better selectivity in the species produced by the reactor. The great majority of microreactors are made of polydimethylsiloxane (PDMS)—a material that cannot operate at elevated pressures or temperatures. Other reported microreactors are made in silicon, ceramics, or metals; although these materials are compatible with high-pressure and high-temperature operation, they have associated a very high production cost because they are made in a semiconductor cleanroom or with specialized, low-throughput tooling, e.g., electro discharge machining.

Hydrogen peroxide (H202), a water-soluble oxidant, spontaneously decomposes in the presence of heat or a catalyst. Applications of a H2O2 catalytic reactor include monopropellant rocket propulsion, steam generators, and pumping; miniaturized versions of such catalytic reactors are of great interest to PowerMEMS. Here, we developed a novel additive manufacturing technique based on silver clay extrusion to create high-pressure compatible and high-temperature compatible, monolithic microfluidics; silver is also a very efficient and effective catalyst for the decomposition of H2O2. Our microreactors are composed of a water-tight microchannel connected to the exterior via two fluidic ports (Figure 1). The experimental performance of the microreactor as a catalytic decomposer of H2O2 matches well our reduced-order modeling estimates (Figure 2), attaining a decomposition efficiency of 87% for a flow rate of 5 µL/min of H2O2 with an initial concentration of 30% w/w. Current research focuses on exploring other applications, e.g., heat exchangers.

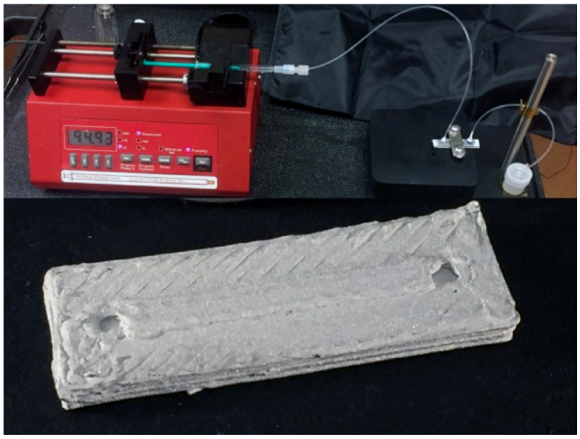

▲Figure 1: Apparatus for experimental characterization of 3D-printed silver catalytic microfluidics using H2O2 (top); 3D-printed, monolithic silver microfluidic with a 350-µm-wide, 2.5-cm-long, and 350-µm-tall microchannel and inlet and outlet fluidic ports (bottom).

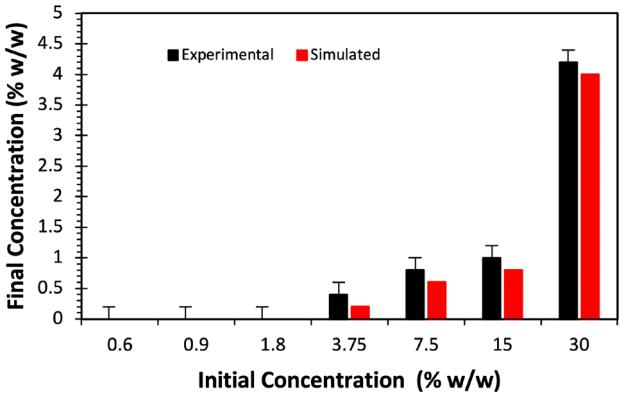

▲Figure 2: Final H2O2 concentration versus initial concentration using a 3D-printed silver microfluidic prototype. Reduced-order modeling simulations and experimental results agree.

FURTHER READING

- Z. Sun, G. Vladimirov, E. Nikolaev, and L. F. Velásquez-García, "Exploration of Metal 3-D Printing Technologies for the Microfabrication of Freeform, Finely Featured, Mesoscaled Structures," *Journal of Microelectromechanical Systems*, vol. 27, no. 6, pp. 1171 – 1185, Dec. 2018.
- F. Eid, L. F. Velásquez-García, and C. Livermore, "Design, Fabrication and Demonstration of a MEMS Steam Generator for Ejector Pump Applications," *Journal of Micromechanics Microengineering*, vol. 20, no. 10, p. 104007, Sep. 2010.
- E. Segura-Cárdenas and L. F. Velásquez-García, "Additively Manufactured Robust Microfluidics via Silver Clay Extrusion," *Journal of Microelectromechanical Systems*, to be published, 2020. DOI: 10.1109/JMEMS.2020.2982559

Management of Brine Effluent from the Desalination Plant

J. Yoon, I. Shrivastava, J. Han
Sponsorship: Kuwait Foundation for the Advancement of Sciences

While large-scale desalination has been a mainstay in a country with a severe water shortage for many decades, management of high concentration brine effluent (> 50,000 TDS) has posed technological, economic, and environmental challenges. There are two research directions to treat the brine effluent effectively: (1) reduce the total volume of effluent onshore and (2) discharge the effluent offshore to minimize environmental impact. Interestingly, the production of effluent is tons of liters, but both studies implement a diffusion process of molecule in the effluent, which appears on a microscopic scale. Here, two technologies are briefly introduced: ion concentration polarization (ICP) to reduce effluent volume and offshore discharge of effluent using plunging liquid jets to minimize environmental impact.

ICP process is a novel electrochemical desalination technology, which emerged within the last decade as a viable option for effluent treatment (Figure 1). ICP employs only a cation exchange membrane (CEM) to utilize a higher diffusivity of chloride (t^(β-)), which is the majority ion in the effluent. Compared with conventional electrochemical desalination such as ED (electrodialysis), it is more energy-efficient, less susceptible to various fouling, and can be implemented with a much smaller footprint. Our group has developed and matured the technology over the years to realize the first-ever lab-scale ICP desalination prototype (~0.1L/min), demonstrating its technical and economic feasibility, and secured several key intellectual properties on this technology.

For the offshore discharge of brine, we are investigating the use of plunging liquid jets (Figure 2) through laboratory experiments. Similar to the widely used offshore discharge outfalls such as submerged or surface jets, plunging jets also utilize the high momentum and negative buoyancy of brine to induce mixing with the surrounding ocean water and reduce the concentration of contaminants such as salt, anti-fouling agents, and anti-scalants that, in turn, reduce the environmental impact. However, unlike these outfalls, plunging jets also introduce air into the water column which, when dissolved, can reduce the environmental impact associated with the creation of hypoxic (low dissolved oxygen) zones.

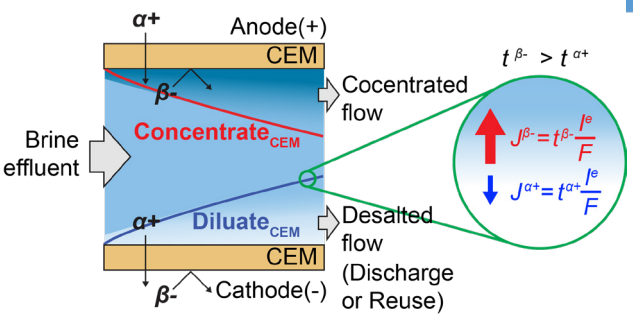

▲ Figure 1: Schematic of ICP process utilizing a higher diffusivity of chloride (t^(β-)).

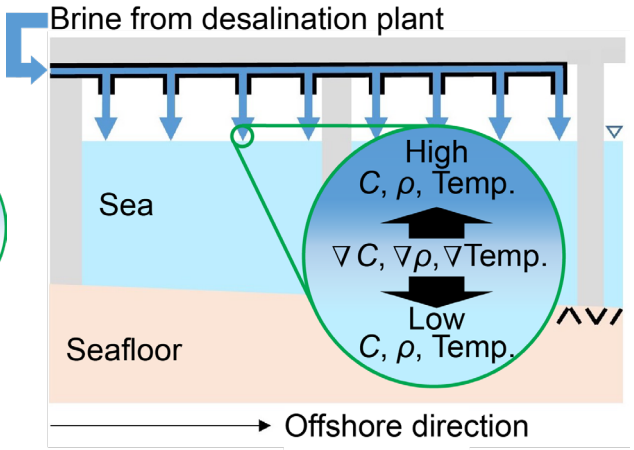

▲ Figure 2: Schematic of offshore discharge using plunging jets.

FURTHER READING

- J. Yoon, V. Q. Do, V.-S. Pham, and J. Han, "Return Flow Ion Concentration Polarization Desalination: A New Way to Enhance Electromembrane Desalination," *Water Research*, vol. 159, pp. 501–510, 2019.
- I. Shrivastava and E. E. Adams, "Pre-dilution of Desalination Reject Brine: Impact on Outfall Dilution in Different Water Depths," *Journal of Hydro-environment Research*, vol. 24, pp. 28-35, 2019.

Reduced-order Modeling of Oil Transport in Internal Combustion Engines Based on Autoencoder

W. Zhang, T. Tian, L. Daniel
Sponsorship: Lubrication in Internal Combustion Engines Consortium in MIT Sloan Automotive Lab

Reducing emissions of internal combustion engines is the major focus in the modern automotive industry. Lubrication oil leakage from the piston ring pack is critical to oil consumption and emission. The oil transport mechanism is not well understood due to the computational complexity of the oil motion and ring pack dynamics and experimental difficulty. This raises our interest to build a reduced-order model predicting the oil movement inside the ring pack with acceptable accuracy and efficiency.

In this work, we proposed a neural-network-based method to perform model order-reduction (MOR) on the computational fluid dynamics (CFD). First, we use a variational autoencoder (VAE) to address the reduce basis of the fluid field and encode the original space into the reduced space. Second, we apply a recurrent neural network (RNN) to learn the dynamics of the reduced space. To guarantee the stability of system dynamics, certain physics-based conservation law and stability regularization are included in the loss function. This method can reduce the fluid dynamics model calculation time by orders of magnitude with acceptable accuracy for analysis. With the reduced-order oil transport model coupled with the piston ring dynamics model, we can quantitatively analyze the mechanisms for oil leakage and inspire design optimization in automotive industry.

The methodology developed in the work is not limited to fluids. The same procedures are applicable to other physical system modeling. Further, the methodology can interpret the neural network behavior from the perspective of model order-reduction.

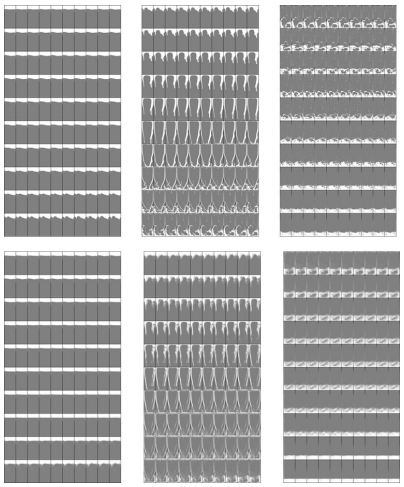

▲ Figure 1: Snapshots of oil dropping inside piston groove (upper row: CFD results, lower row: MOR results with 4 reduced orders.)

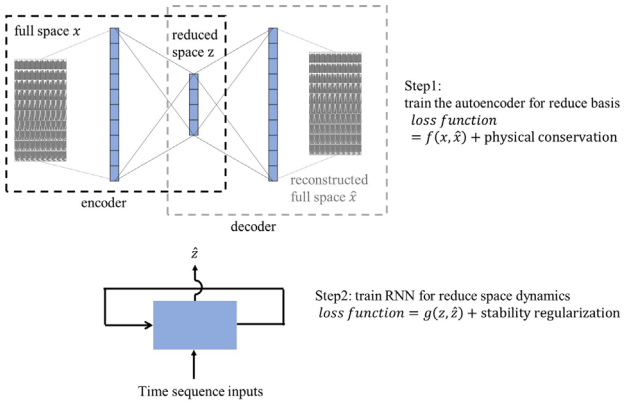

▲ Figure 2: Schematic of neural-network-based MOR.